

MyPortrait: Morphable Prior-Guided Personalized Portrait Generation

Bo Ding^{1,2} Zhenfeng Fan^{1,2} Shuang Yang^{1,2} Shihong Xia^{1,2}

¹Institute of Computing Technology, Chinese Academy of Sciences

²University of Chinese Academy of Sciences

{dingbo21s, fanzhenfeng, yangshuang21b, xsh}@ict.ac.cn

Abstract

Generating realistic talking faces is an interesting and long-standing topic in the field of computer vision. Although significant progress has been made, it is still challenging to generate high-quality dynamic faces with personalized details. This is mainly due to the inability of the general model to represent personalized details and the generalization problem to unseen controllable parameters. In this work, we propose Myportrait, a simple, general, and flexible framework for neural portrait generation. We incorporate personalized prior in a monocular video and morphable prior in 3D face morphable space for generating personalized details under novel controllable parameters. Our proposed framework supports both video-driven and audio-driven face animation given a monocular video of a single person. Distinguished by whether the test data is sent to training or not, our method provides a real-time online version and a high-quality offline version. Comprehensive experiments in various metrics demonstrate the superior performance of our method over the state-of-the-art methods. The code will be publicly available.

1. Introduction

The goal of talking face generation is to generate realistic talking faces whose motion is consistent with the control signals (commonly face video or speech audio), which is a long-standing topic with promising applications in digital human generation, film production, and video dubbing [7, 38, 57, 63]. Recently, significant progress has been made in existing works on neural portrait generation with the advancement of deep learning technologies. Some sophisticated methods are able to generate fake videos which are hardly distinguishable from the real ones.

Existing works on neural portrait generation can be categorized into 2D-based and 3D-based methods. On the one hand, 2D-based methods [18, 34, 40, 49] directly process the image without resorting to facial semantic information (e.g. pose and expression). These methods are user-friendly

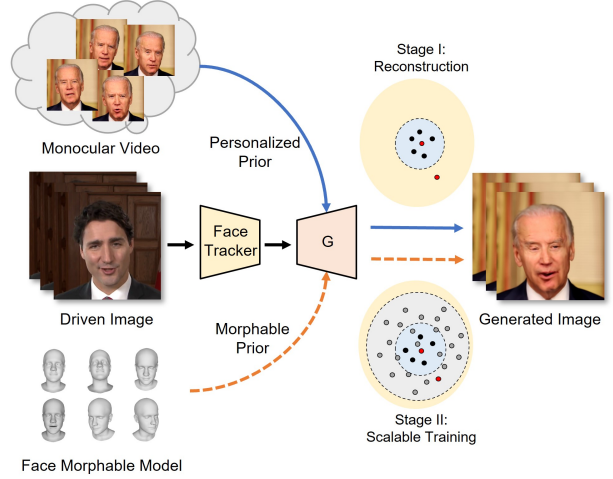


Figure 1. The proposed framework for neural portrait generation. In contrast to previous methods, we explicitly define personalized details in a monocular video as personalized prior. We also introduce a morphable prior in addition to the personalized prior for the generation of high-quality talking faces.

and easy to operate. However, 2D-based methods commonly neglect out-of-plane facial motions and are suboptimal in dealing with pose and expression variations. On the other hand, 3D-based methods [14, 30, 37, 46, 47, 53] generate facial movements from 3D semantic information, e.g. pose and expression parameters from 3D morphable models (3DMM) [3, 4, 28, 36]. These methods achieve flexible control of facial motion but commonly require complex network structures and expensive training costs. Some state-of-the-art methods [43, 55] require a universal facial generator in addition to an input monocular video to recover missing pixels for unseen poses and expressions. As a side effect, a universal generator, e.g. StyleGAN [21–23] and EG3D [5], cannot match personalized characters and generally leads to the degradation of image quality, e.g. missing high-frequency details in the results.

In this work, we study the problem of realistic talking face generation given only a monocular video of an ac-

tor and an input control signal. We develop our proposed method upon the existing 3D-based methods [9, 11, 25, 48], which achieve significant progress in terms of realism and controllability. The key insight is that a monocular video contains abundant information for face reenactment for a person, such as fine textures in various poses, expressions, and phonemes. We explicitly define the facial information in a monocular video as **personalized prior**. Despite the impressive progress of the existing methods, a person’s monocular video usually contains limited 3D semantic parameters (*e.g.* pose and expression) such that the quality of generated faces is not guaranteed for novel parameters.

We further introduce a **morphable prior**, *i.e.* facial shape prior in the format of 3DMM to tackle the generalization problem to novel parameters. Previous works [3, 4, 28, 36] demonstrate that the 3DMM can capture a large percentage of shape variations of 3D facial shapes with only a few linear bases (principal components). In this way, expressions can be decoupled with identities and poses. The morphable prior provides diverse 3D semantic parameters (*e.g.* pose and expression) that mimic the parameters of faces in real scenes and is thus helpful for the generation of novel parameters. This also broadens the expressiveness of the trained models and enhances the quality of the generated videos.

The aforementioned priors motivate us to propose **My-Portrait**, a novel prior-guided framework for neural portrait generation, as shown in Fig. 1. In addition to the personalized prior which is obtained from a monocular video of a single person, we get the morphable prior from auxiliary data in real-life videos. We consider that these auxiliary data contain sufficient 3D semantic parameters for training. Our proposed framework supports both video-driven and audio-driven applications without altering the trunk network structure. Distinguished by whether to send the test data in training, we include an **online** and an **offline** version of our method. The online method can generate images in real-time, while the offline method can greatly improve the generation quality over the existing works. We conduct comprehensive experiments on various datasets to demonstrate the superiority of our proposed framework. In summary, our main contributions are as follows:

- We design a simple, general, and flexible framework for neural portrait generation, which supports both video-driven and audio-driven facial animation given a monocular video of a person.
- We propose a novel prior-guided training strategy for personalized portrait generation with realistic details, which firstly combines personalized prior from a monocular video and morphable prior from face morphable space.
- Comprehensive experiments demonstrate that our method improves the quality of generation over the state-of-the-art methods.

2. Related work

2.1. Neural Portrait Generation

2D-based methods. Several 2D-based methods [34, 39, 41, 50, 62] achieve facial pose and expression transfer by performing warping at the image or feature level. For instance, FOMM [40] is an early method that employs motion field-based image warping to achieve motion transfer without requiring any annotation or prior information about the specific object to be animated. DaGAN [18] recovers dense 3D geometry for talking head video generation. LIA [49] employs self-supervised autoencoders to animate images by navigating in the latent space. Although only one image for the input is required in these methods, they are difficult to recover personalized facial details due to the lack of complete 3D face information in a single image.

3D-based methods. Several 3D structural-based methods [14, 25, 37, 53, 64] use 3D morphable model [3, 4, 28, 36] for portrait generation. Among them, the monocular video-based portrait generation is a mainstream approach. DVP [25] proposes a generative neural network with a novel spatio-temporal architecture that enables realistic re-animation of portrait videos using a single input video. Ner-Face [11] introduces dynamic neural radiation fields for modeling the appearance and dynamics of faces. StyleAvatar [48] proposes a real-time realistic portrait avatar reconstruction method using the StyleGAN [21]. Unlike the complex processing steps of the above methods, DNP [9] proposes a simple 2D coordinate-based multi-layer perceptron (MLP) architecture that learns the mapping from face parameter space to images, which generates controllable dynamic neural portraits. Although the above methods introduce 3DMM, the parameter space is limited in a monocular video. It leads to a degradation of the generation quality when encountering unseen face parameters. To alleviate the difficulty, we introduce a general morphable prior to enrich the face parameters space for training. The quality of the resulting videos is enhanced notably.

2.2. Generative Model and Personalization

Several methods [2, 29, 43, 55, 58] leverage universal generative models to repair missing facial details for reenactment. For instance, StyleHEAT [55] utilizes a pre-trained StyleGAN [21–23] model to enable high-resolution controllable talking face generation. Next3D [43] employs a pre-trained EG3D [5] model to create a 3D-aware head avatar. These methods obtain fine-grained control over face motion but suffer from missing personalized facial details. To address this limitation, Mystyle [32] uses a small number of portrait images of a specific person to fine-tune the weights of the pre-trained StyleGAN face generator, thereby forming a local, low-dimensional, and personalized space in the latent space. Mystyle++ [56] further proposes an approach

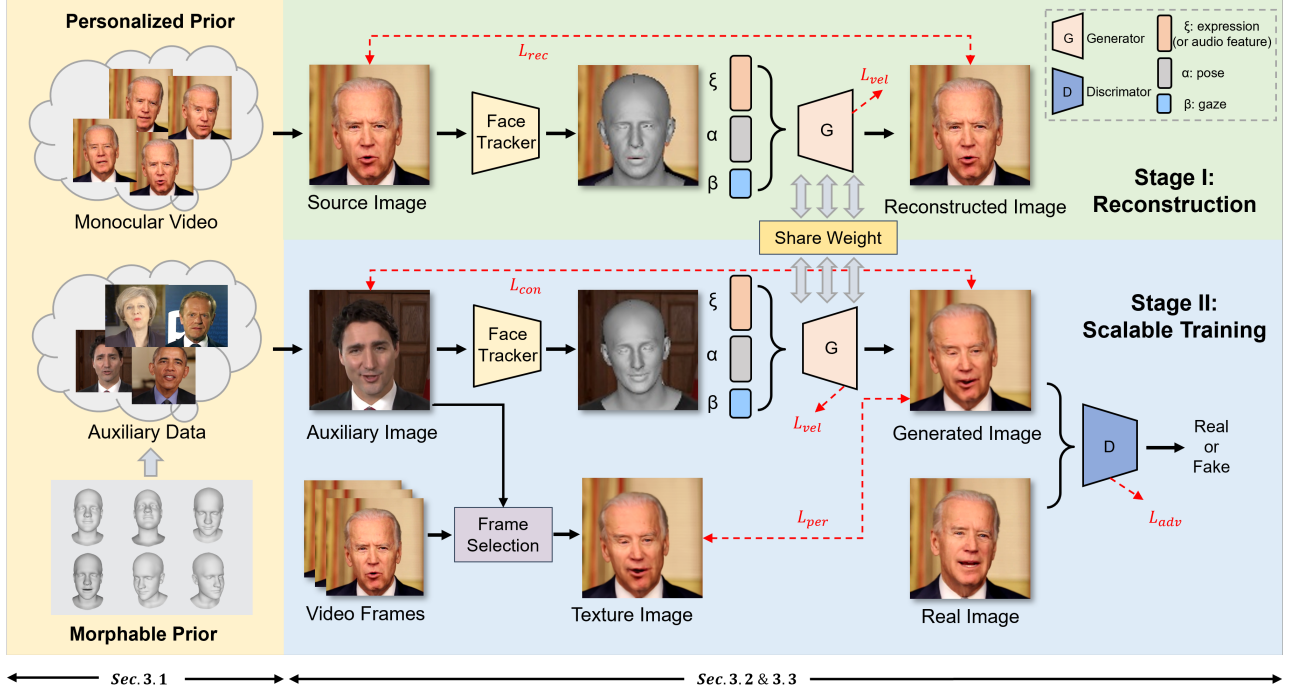


Figure 2. The overview of our method. The network first learns to reconstruct facial images from specific face parameters for a monocular video. The learned face parameter space is then extended by a scalable training strategy, which renders the method capable of generating personalized neural portraits under novel parameters.

to obtain a personalized generative prior with explicit control over a set of attributes. These methods utilize the latent space of a pre-trained generative model for better fine-grained face details. In this work, our method introduces a similar strategy for fine-tuning the results at test time. In a departure from the existing works, we extend the face parameter space by a morphable prior in training for better generalization performance. The architecture of our method is also different from the Mystyle [32] and Mystyle++ [56].

3. Method

In this section, we first introduce two priors for portrait generation, including the personalized prior and the morphable prior. Then, our efficient network structure and loss functions are presented. Finally, we elaborate the training strategy for personalized portrait generation. An overview of our method is presented in Fig. 2.

3.1. Priors for portrait generation

Personalized Prior. Some existing methods [9, 11, 25, 48] use the rich prior information of faces, such as finely textured details under different poses, expressions, and phonemes in a monocular video to generate realistic talking faces. Due to the powerful learning capacity of deep neural networks, these methods are able to generate fake faces that are indistinguishable from real ones. The key to success

is that a monocular video contains all the detailed texture information, both globally and locally for a person under various controllable parameters, *e.g.* expressions in video-driven facial animations and phonemes in audio-driven facial animations. The texture information can be stored in the weights of a well-trained network to repair the missing facial details in certain semantics. In this work, we explicitly define the detailed texture information in a monocular video as *personalized prior*.

Morphable Prior. Our goal is to generate realistic facial videos of a person under various semantics which are related to varying shapes and poses of a face. The deformation of shapes is commonly caused by expressions and phonemes, depending on video-driven and audio-driven applications, respectively. Taking the video-driven applications as an example¹, we define the morphable parameter space of all possible poses and expressions of a single person as \mathcal{M} . We call this the *morphable prior* coupled with the high-level semantics.

Ideally, we hope that a trained model for a monocular video is generalizable to all possible semantic parameters. However, this is not achievable due to the limited semantics of a monocular video in practical applications. We define the limited parameter space provided in the monocular

¹We can replace the expressions by the phonemes in audio-driven applications.

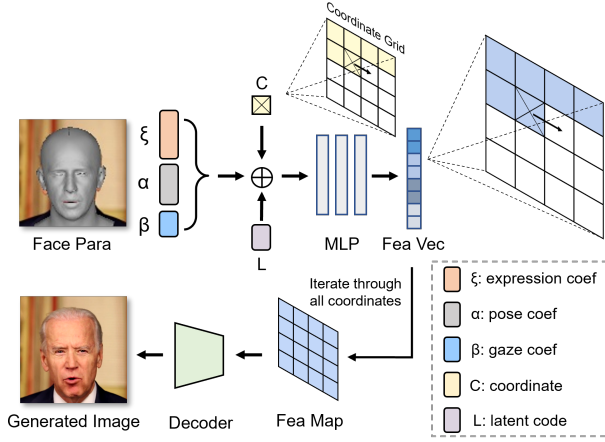


Figure 3. The illustration of the generator network. The generator consists of a 2D coordinate-based MLP and a CNN-based decoder.

video as \mathbf{S} , which is smaller than \mathbf{M} , as

$$\mathbf{S} \subset \mathbf{M}. \quad (1)$$

Most existing models [14, 48, 64] can only animate the input parameters in the subspace \mathbf{S} . The generation quality is commonly degraded for unseen input parameters in \mathbf{M}/\mathbf{S} . To overcome this limitation, we introduce a universal facial prior in terms of the poses and expressions of the 3DMM [3, 4, 28, 36]. The prior captures general domain knowledge about facial shape variations, which allows any face to be represented as a linear combination of a finite basis set of face prototypes. We then sample the morphable parameter space in \mathbf{M} to extend the input parameter space \mathbf{S} . The extended parameter space are denoted by \mathbf{S}' . Finally, the trained model can generate high-quality videos in the extended parameter space \mathbf{S}' , which approaches the ideal morphable parameter space \mathbf{M} , as

$$\mathbf{S} \subset \mathbf{S}' \rightarrow \mathbf{M}. \quad (2)$$

The process is illustrated in Fig. 4.

In our implementation, we sample the morphable parameters from real-life videos with a state-of-the-art 3D reconstruction method [10]. We call these real-life videos as *auxiliary data*, which provides not only various morphable parameters but also temporal sequences for training. After all, the frames from auxiliary data contain smoothly varying parameters and contribute to temporally coherent results. In addition, the extended parameter space \mathbf{S}' approaches the ideal morphable space \mathbf{M} as the auxiliary data increase.

3.2. Network structure and loss functions

We use a simple 2D coordinate-concatenated MLP and CNN-based decoder network architecture of which the main branch is similar to the DNP [9]. This considers the training

efficiency in case of the increase of auxiliary data compared to a monocular video. Unlike DNP, we use bilinear interpolation rather than transposed convolution for upsampling because we observe that transposed convolution produces checkerboard artifacts [33]. This also reduces the computational cost. We utilize per-image learnable latent code to model information in the image that is difficult to describe in terms of face parameters, including factors such as facial details, bodily motion, and illumination changes. Besides the pose and expression parameters of the 3DMM, we introduce gaze as an input parameter to control the gaze angle of the generated image in video-driven tasks. The structure of the generator is illustrated in Fig. 3. In addition, we also include three auxiliary networks in training to enhance the generation quality. Firstly, we adopt a patch-based GAN architecture [13, 19, 65] to force the generated faces to be indistinguishable to truth faces. Secondly, we employ the pre-trained VGGNet [20, 42] for adding perceptual loss as a common routine in low-level feature generation methods [2, 48]. Finally, we also include a feature extraction network for parameter consistency between the generated face and the driven one.²

Loss Function. A variety of loss functions are carefully designed to train the network efficiently, as follows (also refer to Fig. 2).

(a) *Reconstruction loss* ensures the generated image $G(c)$ to match the ground truth image y as

$$L_{rec} = \|y - G(c)\|_2, \quad (3)$$

where G denotes the generator network taking the face parameter c as input.

(b) *Perceptual loss* ensures semantic feature consistency between the generated image and the ground truth image as

$$L_{per} = \sum_{i=1}^I \|N_i(t) - N_i(G(c))\|_1, \quad (4)$$

where $N_i(\cdot)$ represents the i^{th} channel feature extracted from a specific VGG-19 layer, t is the texture image obtained by performing frame selection based on the nearest neighbor of the face parameter, and I is the number of feature channels in this layer.

(c) *Consistency loss* ensures face parameters (e.g. expressions, and poses) consistency between the generated face and the driven one, as

$$L_{con} = \|c - \Phi(G(c))\|_2, \quad (5)$$

where we implement $\Phi(\cdot)$ with the DECA [10] model.

(d) *Adversarial loss* consists of two components: L_{adv}^D for the discriminator and L_{adv}^G for the generator to force the

²The details for the network structure are included in the supplementary material.

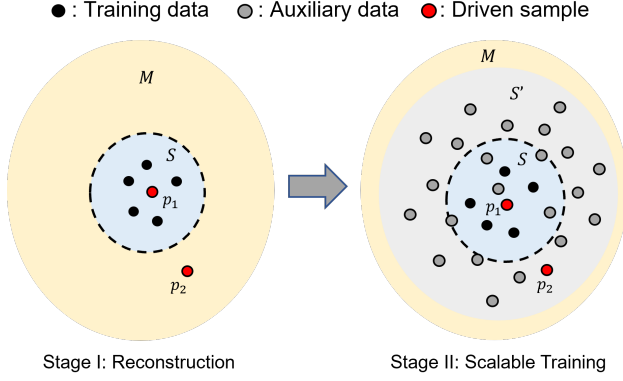


Figure 4. Variations of face parameter space for two training stages. In the first stage, the network learns personalized prior from a monocular video. In the second stage, we introduce morphable prior to extend the face parameter space. p_1 and p_2 show two examples which are inside and outside the original parameter space S of the input monocular video, respectively. After the second stage, p_2 is covered by the extended parameter space S' .

distribution of generated images to align with the real ones as:

$$L_{adv}^D = \log(D(G(c))) + \log(1 - D(y)), \quad (6)$$

and

$$L_{adv}^G = \log(1 - D(G(c))). \quad (7)$$

(e) *Velocity loss* ensures coherence between adjacent frames as

$$L_{vel} = (\|v_i\|_2 + \|v_{i+1}\|_2) + \|v_i - v_{i+1}\|_2, \quad (8)$$

where i represents the i^{th} frame, and v_i and v_{i+1} represent the corresponding latent codes of the adjacent frames. The two terms in Eq. (8) encourage sparsity and temporal consistency of the latent code, respectively.

Finally, the full objective functions are

$$L_D = L_{adv}^D, \quad (9)$$

and

$$L_G = L_{adv}^G + \alpha_1 L_{rec} + \alpha_2 L_{per} + \alpha_3 L_{con} + \alpha_4 L_{vel}, \quad (10)$$

for the discriminator and the generator, respectively. Here, α_1 , α_2 , α_3 , and α_4 are weights for different terms.

3.3. Prior-guided training strategy

In this section, we propose a prior-guided *two-stage* training strategy to effectively make use of the aforementioned two priors for personalized portrait generation with high-quality details.

Stage I: Reconstruction Training. In the first stage, we perform reconstruction training on a monocular video.

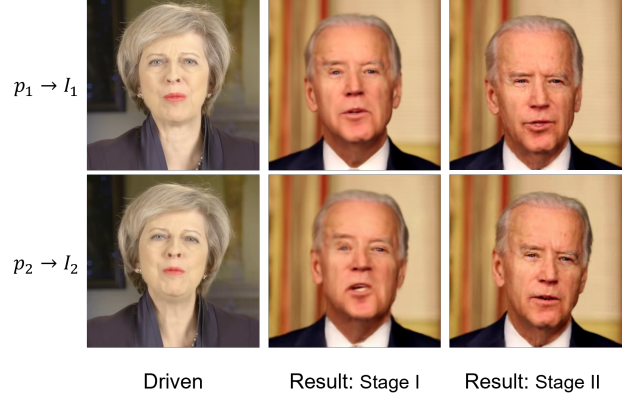


Figure 5. Two examples (also refer to Fig. 4) for p_1 and p_2 for neural portrait generation in the two stages. The top examples show good reconstruction in the first stage. The bottom examples show some artifacts in the first stage, such as the inaccurate mouth and blurred eyes, while they are well-fixed by the second stage.

Specifically, we use a face tracker to extract face parameters in the monocular video. We employ DECA [10] and DeepSpeech [1, 16] for video-driven and audio-driven tasks as the face tracker, respectively. The output parameters (expressions, poses, or phonemes) of the face tracker are used as the input parameters of our network. During this training stage, we only use the reconstruction loss in Eq. (3) and the velocity loss in Eq. (8).

Now our goal is to learn personalized details from the monocular video, in which we explicitly define the information as the personalized prior. During training, the mapping of different face parameters to reconstructed images is learned. Benefiting from a fixed identity and background, the monocular video can recover the personalized details of the given identity. Meanwhile, the irrelevant content, such as the identity and background, remains unchanged. Fig. 5 shows two examples inside and outside the parameter space of the monocular video, respectively (also refer to p_1 and p_2 in Fig. 4). The limitation is that the generation quality is not guaranteed for novel parameters that are located outside the parameter space S of the monocular video.

Stage II: Scalable Training. In the second stage, we aim to incorporate the morphable prior into training for generating realistic faces with novel parameters. We extract face parameters from auxiliary data and feed them into training.

Our purpose now is to generate high-quality faces even if the parameter is not included in the monocular video. Since the novel parameters are provided by auxiliary data, the corresponding ground truth images for the identity in the monocular video are missing. In this stage, the loss terms in Eqs. (4) to (7), together with the auxiliary networks are employed for the novel parameters extracted from auxiliary data. As a result, the trained network is capable of fix-

Method	Portrait	L1(↓)	LPIPS(↓)	FID(↓)
FOMM [40]	ID.1	0.052	0.078	54.184
	ID.2	0.063	0.134	137.60
	ID.3	0.039	0.090	79.780
NerFACE [11]	ID.1	0.037	0.056	63.514
	ID.2	0.048	0.118	102.26
	ID.3	0.023	0.025	41.268
DNP [9]	ID.1	0.046	0.112	23.975
	ID.2	0.032	0.081	20.834
	ID.3	0.020	0.040	21.536
Ours	ID.1	0.045	0.102	15.441
	ID.2	0.031	0.073	16.920
	ID.3	0.020	0.037	17.894

Table 1. Comparison to self-reenactment methods on the NerFace dataset. The bold results are the best.

ing the missing details conditioned on the novel parameters, thereby improving the quality of generated faces notably as in Fig. 5 (the bottom example).

Fig. 4 and Fig. 5 also show that the parameter space is broadened after scalable training, as our desired effect by the introduction of the proposed morphable prior. In practice, we can extract the semantic parameters of the driven video and feed them into scalable training. We find that the quality of the generated faces is greatly enhanced in this way. This is in fact a similar strategy for fine-tuning the results at test time [12, 44] at the cost of sacrificing real-time performance. We distinguish our proposed method by an **online** version and an **offline** version based on whether to send the test data in training. The online method can generate images in real-time, while the offline method can greatly improve the generation quality over existing works.

4. Experiments

4.1. Experiment Setup

Dataset. Our approach trains neural portraits on monocular videos, creating a new model for each identity-specific video. The experimental data come from Head2Head [8, 27] and NerFACE [11]. We extract and store the expression, pose, phoneme, and gaze parameters of the facial videos for data preprocessing. We also pre-crop the face images for the actor in the monocular video, keeping a fixed background and camera viewpoint. Please refer to the supplementary material for more details.

Metric. Referring to existing monocular video-based methods [9, 11, 25, 48], we evaluate the performance of our method in self-reenactment and cross-reenactment experiments. In the self-reenactment experiment, we use L1-distance (L1) and Learned Perceptual Image Patch Similarity (LPIPS) [60] to quantitatively assess the portrait reconstruction with respect to ground truths. Additionally, we use the Frechet Inception Distance (FID) [17], a met-

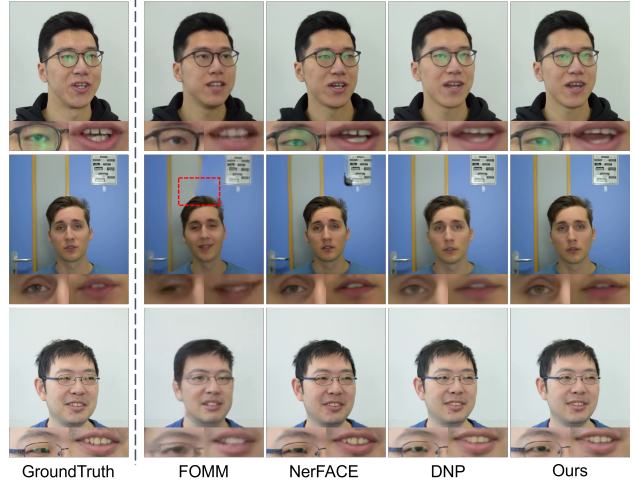


Figure 6. Visual comparison to self-reenactment methods. Please zoom in to see the details.

ric for the realism of generated images to evaluate the difference between the feature distributions of generated and real images. In the cross-reenactment experiment, Cosine Similarity (CSIM) of identity embedding is used to assess the preservation of the target’s identity information in the generated images, with the assistance of ArcFace [6]. Furthermore, we refer to PIRender [37] to assess the semantic consistency of the driven signal using the Average Expression Distance (AED) and the Average Pose Distance (APD).

4.2. Comparison to the State of the Art

We compare the performance of our method with state-of-the-art methods, including FOMM [40], StyleHEAT [55], NerFACE [11], and DNP [9]. FOMM and StyleHEAT are 2D-based methods for face reenactment based on a single reference image. NerFACE and DNP are 3D-based methods that leverage a monocular video to generate neural portraits.

Self-Reenactment. We conduct self-reenactment experiments on the NerFace dataset to compare with the existing methods. The quantitative experimental results are presented in Tab. 1. Compared to state-of-the-art methods, our method achieves superior performance in all metrics. The reconstruction loss allows us to achieve a lower L1 distance. Additionally, by optimizing the perceptual loss and the adversarial loss, the feature distribution of the images generated by our method aligns better with that of the real images, resulting in a lower LPIPS and FID. Visual comparison with self-reenactment methods is illustrated in Fig. 6. FOMM [40] uses only one reference image for motion transfer, leading to the lack of facial prior in the generated images. The warping strategy based on the motion field also causes distortions in the background, as shown by the red box in Fig. 6, middle row. NerFACE [11] assumes that the head

Method	Target: Biden Driven: May				Target: Trudeau Driven: tusk				Target: May Driven: Trudeau			
	CSIM(\uparrow)	APD(\downarrow)	AED(\downarrow)	FID(\downarrow)	CSIM(\uparrow)	APD(\downarrow)	AED(\downarrow)	FID(\downarrow)	CSIM(\uparrow)	APD(\downarrow)	AED(\downarrow)	FID(\downarrow)
StyleHEAT [55]	0.358	0.014	0.184	61.285	0.381	0.015	0.253	93.360	0.158	0.028	0.209	132.704
DNP [9]	0.278	0.011	0.200	23.964	0.385	0.015	0.288	116.512	0.508	0.030	0.252	96.323
Ours (online)	0.327	0.015	0.204	22.500	0.573	0.028	0.416	30.429	0.664	0.039	0.275	68.745
Ours (offline)	0.514	0.012	0.214	8.553	0.634	0.018	0.291	5.513	0.749	0.033	0.203	15.590

Table 2. Comparison to cross-reenactment methods on the Head2Head dataset. The bold results are the best.



Figure 7. Visual comparison to cross-reenactment methods. Please zoom in to see the details.

pose parameters are consistent with the camera viewpoints, resulting in inconsistencies in the generated torsos. DNP [9] achieves good performance in terms of generation quality after simplifying 3D to 2D scenes. However, it is limited by the different distributions of training and testing data, which results in missing facial details in the generated images. In contrast, our method introduces morphable prior to extend the face parameter space in training, thus greatly improving the generation quality.

Cross-Reenactment. We also conduct cross-reenactment experiments on the NerFace dataset to compare with the existing methods. It should be noted that cross-reenactment is more difficult than self-reenactment for monocular video-based portrait generation methods. The training data and testing data of cross-reenactment come from different identities, which causes significant differences in the face parameter distributions. Tab. 2 shows the results of the quantitative experiments on cross-reenactment. Our offline method achieves the best CSIM and FID under various experimental settings. It should be noted that our method aligns the generated images to the real ones at the expense of certain face parameter consistency, which causes our method to be slightly worse than StyleHEAT [55] in terms of APD and AED, but with higher generation quality. The visual comparison with the cross-reenactment methods is presented in Fig. 7. Although StyleHEAT [55] uses universal face prior from other datasets to recover facial details, the lack of personalized prior makes it difficult to gener-

Method	L1(\downarrow)	LPIPS(\downarrow)	FID(\downarrow)
SadTalker [61]	0.106	0.365	86.517
DNP [9]	0.035	0.074	17.601
Ours	0.035	0.065	10.880

Table 3. Comparison to audio-driven reenactment methods. The bold results are the best.

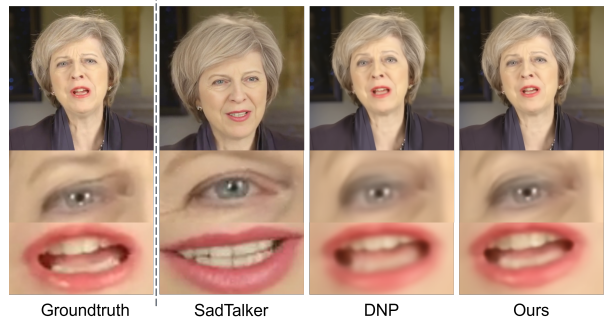


Figure 8. Visual comparison to audio-driven methods. Please zoom in to see the details.

ate personalized facial images. Affected by the inconsistent distribution of face parameters between the training and driving data, unexpected artifacts appear in the generated images with DNP [9]. Our online method mitigates this situation after introducing morphable prior. Further, after including the driven data in training, our offline method generates portraits with significantly improved quality.

Audio-driven Reenactment. Existing audio-driven face reenactment methods [51, 52, 54, 61] have made significant progress. Although our framework makes improvements primarily for the video-driven method, it also achieves certain performance gains for the audio-driven applications. We include SadTalker [61] and DNP [9] for comparison. SadTalker is an advanced method for generating a realistic video of a talking face based on an input piece of audio and a face image. DNP can also be used for audio-driven tasks. Quantitative results are shown in Tab. 3. SadTalker, despite its ability to generate a better lip-synchronized video with the help of facial information learned from a large amount of data, is limited by the lack of information about the target face, resulting in the inability to portray personalized details. Overall, our method achieves the best generation

Method	CSIM(\uparrow)	APD(\downarrow)	AED(\downarrow)	FID(\downarrow)
wo L_{gan}	0.437	0.025	0.255	13.265
wo L_{per}	0.459	0.022	0.260	11.819
wo L_{con}	0.458	0.024	0.255	10.376
wo L_{vel}	0.469	0.026	0.229	10.758
Ours (full)	0.461	0.026	0.237	10.713

Table 4. Ablation study of loss functions. The best performance is highlighted in **red** (1st best) and **blue** (2nd best).

quality. Fig. 8 presents qualitative results, suggesting that the morphable prior introduced via 3DMM is valid for improving the result of audio-driven reenactment.

4.3. Ablation Study

To assess the impact of different components of our method associated with loss items, we remove each term in the loss function and evaluate the influence in the cross-reenactment experiment. The quantitative results are shown in Tab. 4. It can be observed that the adversarial loss L_{gan} and the perceptual loss L_{per} play major roles in the generation process as their removal causes an overall degradation in the generation quality. In addition, the consistency loss L_{con} helps to keep the face parameters consistent between the generated and driven images. Finally, the removal of the velocity loss L_{vel} results in a slightly worse quality, which is due to the correlation of facial details between adjacent frames of a video. In general, our method exhibits superior performance benefiting from well-designed loss functions.

In order to assess the impact of the size of the face parameter space provided by the morphable prior, we gradually increase the number of videos k in the auxiliary data and test our method in a cross-reenactment experiment. Considering the inability to accurately measure the difference in face parameter diversity between videos, we chose to add one video at a time to the auxiliary data. The quantitative results are shown in Tab. 5. It can be observed that the generation quality improves as the size of auxiliary data increases. This suggests that the full morphable prior space can be approached as the size of the auxiliary data increases.

4.4. Feature Visualisation

In order to compare the structural differences of the face parameters before and after the scalable training stage, we use t-SNE [45] to visualize the expression and pose coefficients, respectively. There are three categories of face parameters shown in Fig. 9, the monocular video used for training (Performing data, red dots), the face parameters corresponding to stage I (yellow dots), and the face parameters corresponding to the images generated by stage II (blue dots). It can be observed that in both Fig. 9 (a) and Fig. 9 (b), the yellow dots are far away from the red dots, while the blue dots are entangled with the red dots. The driven data in stage II

Method	CSIM(\uparrow)	APD(\downarrow)	AED(\downarrow)	FID(\downarrow)
Ours ($k = 0$)	0.403	0.028	0.245	23.700
Ours ($k = 1$)	0.441	0.029	0.325	12.652
Ours ($k = 2$)	0.456	0.027	0.247	11.156
Ours ($k = 3$)	0.461	0.026	0.237	10.713

Table 5. Ablation study for gradually adding the number of videos in the auxiliary data. The bold results are the best.

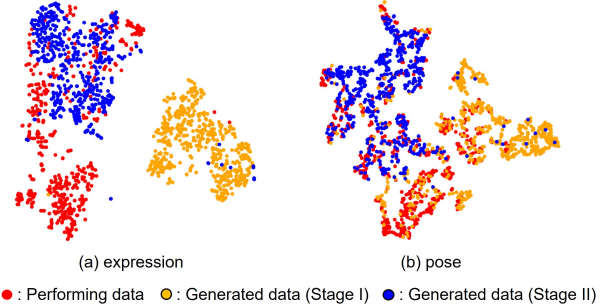


Figure 9. Visualisation of face parameters before and after the scalable training stage.

are forced to align with the performing data. This suggests that our training strategy, by introducing the auxiliary data, helps to mitigate the effects caused by the different distribution between the training and testing data. In addition to the personalized prior provided by a monocular video, we introduce the morphable prior to enhance the expressiveness of the trained model, resulting in high-quality personalized details under various semantic parameters.

5. Conclusion and Discussion

Conclusion. In this work, we present MyPortrait, a simple, general, and flexible framework for neural portrait generation. By exploiting personalized prior from a monocular video and morphable prior provided by 3DMM, our framework generates high-quality personalized dynamic faces. Comprehensive experiments demonstrate that our method outperforms the state-of-the-art ones. This work provides a novel perspective in generating personalized details for future research on face reenactment.

Limitation. Benefiting from the reduction of 3D to 2D scenes, our method can be trained using a simple network structure. However, this also results in that our method can only be applied to monocular videos with fixed backgrounds. It is promising to combine our method with face segmentation methods in the future. In addition, the accuracy of face parameters extracted by face trackers greatly influences our method’s performance. With the development of face trackers, the performance of our method will be further improved.

References

- [1] Dario Amodei, Sundaram Ananthanarayanan, Rishita Anubhai, Jingliang Bai, Eric Battenberg, Carl Case, Jared Casper, Bryan Catanzaro, Qiang Cheng, Guoliang Chen, et al. Deep speech 2: End-to-end speech recognition in english and mandarin. In *International Conference on Machine Learning*, pages 173–182, 2016. 5, 1, 2
- [2] Yunpeng Bai, Yanbo Fan, Xuan Wang, Yong Zhang, Jingxiang Sun, Chun Yuan, and Ying Shan. High-fidelity facial avatar reconstruction from monocular video with generative priors. In *Proceedings of the IEEE/CVF Conference on Computer Vision and Pattern Recognition*, pages 4541–4551, 2023. 2, 4
- [3] Volker Blanz and Thomas Vetter. A morphable model for the synthesis of 3d faces. In *Proceedings of the 26th annual conference on Computer graphics and interactive techniques*, pages 187–194, 1999. 1, 2, 4
- [4] James Booth, Anastasios Roussos, Stefanos Zafeiriou, Allan Ponniah, and David Dunaway. A 3d morphable model learnt from 10,000 faces. In *Proceedings of the IEEE conference on Computer Vision and Pattern Recognition*, pages 5543–5552, 2016. 1, 2, 4
- [5] Eric R Chan, Connor Z Lin, Matthew A Chan, Koki Nagano, Boxiao Pan, Shalini De Mello, Orazio Gallo, Leonidas J Guibas, Jonathan Tremblay, Sameh Khamis, et al. Efficient geometry-aware 3d generative adversarial networks. In *Proceedings of the IEEE/CVF Conference on Computer Vision and Pattern Recognition*, pages 16123–16133, 2022. 1, 2
- [6] Jiankang Deng, Jia Guo, Niannan Xue, and Stefanos Zafeiriou. Arcface: Additive angular margin loss for deep face recognition. In *Proceedings of the IEEE/CVF Conference on Computer Vision and Pattern Recognition*, pages 4690–4699, 2019. 6
- [7] Sourabh Dhere, Suresh B Rathod, Sanket Aarankalle, Yash Lad, and Megh Gandhi. A review on face reenactment techniques. In *2020 International Conference on Industry 4.0 Technology*, pages 191–194. IEEE, 2020. 1
- [8] Michail Christos Doukas, Mohammad Rami Koujan, Viktoriia Sharmanska, Anastasios Roussos, and Stefanos Zafeiriou. Head2head++: Deep facial attributes re-targeting. *IEEE Transactions on Biometrics, Behavior, and Identity Science*, 3(1):31–43, 2021. 6, 1
- [9] Michail Christos Doukas, Stylianos Ploumpis, and Stefanos Zafeiriou. Dynamic neural portraits. In *Proceedings of the IEEE/CVF Winter Conference on Applications of Computer Vision*, pages 4073–4083, 2023. 2, 3, 4, 6, 7, 1
- [10] Yao Feng, Haiwen Feng, Michael J Black, and Timo Bolkart. Learning an animatable detailed 3d face model from in-the-wild images. *ACM Transactions on Graphics*, 40(4):1–13, 2021. 4, 5, 1
- [11] Guy Gafni, Justus Thies, Michael Zollhofer, and Matthias Nießner. Dynamic neural radiance fields for monocular 4d facial avatar reconstruction. In *Proceedings of the IEEE/CVF Conference on Computer Vision and Pattern Recognition*, pages 8649–8658, 2021. 2, 3, 6, 1
- [12] Yossi Gandelsman, Yu Sun, Xinlei Chen, and Alexei Efros. Test-time training with masked autoencoders. *Advances in Neural Information Processing Systems*, 35:29374–29385, 2022. 6
- [13] Ian Goodfellow, Jean Pouget-Abadie, Mehdi Mirza, Bing Xu, David Warde-Farley, Sherjil Ozair, Aaron Courville, and Yoshua Bengio. Generative adversarial nets. *Advances in neural information processing systems*, 27, 2014. 4
- [14] Philip-William Grassal, Malte Prinzler, Titus Leistner, Carsten Rother, Matthias Nießner, and Justus Thies. Neural head avatars from monocular rgb videos. In *Proceedings of the IEEE/CVF Conference on Computer Vision and Pattern Recognition*, pages 18653–18664, 2022. 1, 2, 4
- [15] Yudong Guo, Keyu Chen, Sen Liang, Yong-Jin Liu, Hujun Bao, and Juyong Zhang. Ad-nerf: Audio driven neural radiance fields for talking head synthesis. In *Proceedings of the IEEE/CVF International Conference on Computer Vision*, pages 5784–5794, 2021. 2
- [16] Awni Hannun, Carl Case, Jared Casper, Bryan Catanzaro, Greg Diamos, Erich Elsen, Ryan Prenger, Sanjeev Satheesh, Shubho Sengupta, Adam Coates, et al. Deep speech: Scaling up end-to-end speech recognition. *arXiv preprint arXiv:1412.5567*, 2014. 5, 1, 2
- [17] Martin Heusel, Hubert Ramsauer, Thomas Unterthiner, Bernhard Nessler, and Sepp Hochreiter. Gans trained by a two time-scale update rule converge to a local nash equilibrium. *Advances in neural information processing systems*, 30, 2017. 6
- [18] Fa-Ting Hong, Longhao Zhang, Li Shen, and Dan Xu. Depth-aware generative adversarial network for talking head video generation. In *Proceedings of the IEEE/CVF Conference on Computer Vision and Pattern Recognition*, pages 3397–3406, 2022. 1, 2
- [19] Phillip Isola, Jun-Yan Zhu, Tinghui Zhou, and Alexei A Efros. Image-to-image translation with conditional adversarial networks. In *Proceedings of the IEEE/CVF Conference on Computer Vision and Pattern Recognition*, pages 1125–1134, 2017. 4, 2
- [20] Justin Johnson, Alexandre Alahi, and Li Fei-Fei. Perceptual losses for real-time style transfer and super-resolution. In *Proceedings of the European Conference on Computer Vision*, pages 694–711. Springer, 2016. 4
- [21] Tero Karras, Samuli Laine, and Timo Aila. A style-based generator architecture for generative adversarial networks. In *Proceedings of the IEEE/CVF Conference on Computer Vision and Pattern Recognition*, pages 4401–4410, 2019. 1, 2
- [22] Tero Karras, Samuli Laine, Miika Aittala, Janne Hellsten, Jaakko Lehtinen, and Timo Aila. Analyzing and improving the image quality of stylegan. In *Proceedings of the IEEE/CVF Conference on Computer Vision and Pattern Recognition*, pages 8110–8119, 2020.
- [23] Tero Karras, Miika Aittala, Samuli Laine, Erik Härkönen, Janne Hellsten, Jaakko Lehtinen, and Timo Aila. Alias-free generative adversarial networks. *Advances in Neural Information Processing Systems*, 34:852–863, 2021. 1, 2
- [24] Petr Kellnhofer, Adria Recasens, Simon Stent, Wojciech Matusik, and Antonio Torralba. Gaze360: Physically unconstrained gaze estimation in the wild. In *Proceedings of the*

- IEEE/CVF International Conference on Computer Vision*, pages 6912–6921, 2019. 1
- [25] Hyeonwoo Kim, Pablo Garrido, Ayush Tewari, Weipeng Xu, Justus Thies, Matthias Niessner, Patrick Pérez, Christian Richardt, Michael Zollhöfer, and Christian Theobalt. Deep video portraits. *ACM Transactions on Graphics*, 37(4):1–14, 2018. 2, 3, 6
- [26] Diederik P Kingma and Jimmy Ba. Adam: A method for stochastic optimization. In *International Conference on Learning Representations*, 2015. 1
- [27] Mohammad Rami Koujan, Michail Christos Doukas, Anastasios Roussos, and Stefanos Zafeiriou. Head2head: Video-based neural head synthesis. In *2020 15th IEEE International Conference on Automatic Face and Gesture Recognition*, pages 16–23. IEEE, 2020. 6, 1
- [28] Tianye Li, Timo Bolkart, Michael J Black, Hao Li, and Javier Romero. Learning a model of facial shape and expression from 4d scans. *ACM Trans. Graph.*, 36(6):194–1, 2017. 1, 2, 4
- [29] Zhiyuan Ma, Xiangyu Zhu, Guo-Jun Qi, Zhen Lei, and Lei Zhang. Otavatar: One-shot talking face avatar with controllable tri-plane rendering. In *Proceedings of the IEEE/CVF Conference on Computer Vision and Pattern Recognition*, pages 16901–16910, 2023. 2
- [30] Safa C Medin, Bernhard Egger, Anoop Cherian, Ye Wang, Joshua B Tenenbaum, Xiaoming Liu, and Tim K Marks. Most-gan: 3d morphable stylegan for disentangled face image manipulation. In *Proceedings of the AAAI Conference on Artificial Intelligence*, pages 1962–1971, 2022. 1
- [31] Takeru Miyato, Toshiki Kataoka, Masanori Koyama, and Yuichi Yoshida. Spectral normalization for generative adversarial networks. In *International Conference on Learning Representations*, 2018. 2
- [32] Yotam Nitzan, Kfir Aberman, Qiurui He, Orly Liba, Michal Yarom, Yossi Gandelsman, Inbar Mosseri, Yael Pritch, and Daniel Cohen-Or. Mystyle: A personalized generative prior. *ACM Transactions on Graphics*, 41(6):1–10, 2022. 2, 3
- [33] Augustus Odena, Vincent Dumoulin, and Chris Olah. Deconvolution and checkerboard artifacts. *Distill*, 1(10):e3, 2016. 4, 1
- [34] Trevine Oorloff and Yaser Yacoob. Robust one-shot face video re-enactment using hybrid latent spaces of stylegan2. In *Proceedings of the IEEE/CVF International Conference on Computer Vision*, pages 20947–20957, 2023. 1, 2
- [35] Adam Paszke, Sam Gross, Francisco Massa, Adam Lerer, James Bradbury, Gregory Chanan, Trevor Killeen, Zeming Lin, Natalia Gimelshein, Luca Antiga, et al. Pytorch: An imperative style, high-performance deep learning library. *Advances in Neural Information Processing Systems*, 32, 2019. 1
- [36] Pascal Paysan, Reinhard Knothe, Brian Amberg, Sami Romdhani, and Thomas Vetter. A 3d face model for pose and illumination invariant face recognition. In *2009 sixth IEEE international conference on advanced video and signal based surveillance*, pages 296–301. Ieee, 2009. 1, 2, 4
- [37] Yurui Ren, Ge Li, Yuanqi Chen, Thomas H Li, and Shan Liu. Pirenderer: Controllable portrait image generation via semantic neural rendering. In *Proceedings of the IEEE/CVF International Conference on Computer Vision*, pages 13759–13768, 2021. 1, 2, 6
- [38] Tong Sha, Wei Zhang, Tong Shen, Zhoujun Li, and Tao Mei. Deep person generation: A survey from the perspective of face, pose, and cloth synthesis. *ACM Computing Surveys*, 55(12):1–37, 2023. 1
- [39] Aliaksandr Siarohin, Stéphane Lathuilière, Sergey Tulyakov, Elisa Ricci, and Nicu Sebe. Animating arbitrary objects via deep motion transfer. In *Proceedings of the IEEE/CVF Conference on Computer Vision and Pattern Recognition*, pages 2377–2386, 2019. 2
- [40] Aliaksandr Siarohin, Stéphane Lathuilière, Sergey Tulyakov, Elisa Ricci, and Nicu Sebe. First order motion model for image animation. In *Proceedings of the 33rd International Conference on Neural Information Processing Systems*, pages 7137–7147, 2019. 1, 2, 6
- [41] Aliaksandr Siarohin, Oliver J Woodford, Jian Ren, Menglei Chai, and Sergey Tulyakov. Motion representations for articulated animation. In *Proceedings of the IEEE/CVF Conference on Computer Vision and Pattern Recognition*, pages 13653–13662, 2021. 2
- [42] Karen Simonyan and Andrew Zisserman. Very deep convolutional networks for large-scale image recognition. In *International Conference on Learning Representations*, 2015. 4
- [43] Jingxiang Sun, Xuan Wang, Lizhen Wang, Xiaoyu Li, Yong Zhang, Hongwen Zhang, and Yebin Liu. Next3d: Generative neural texture rasterization for 3d-aware head avatars. In *Proceedings of the IEEE/CVF Conference on Computer Vision and Pattern Recognition*, pages 20991–21002, 2023. 1, 2
- [44] Yu Sun, Xinhao Li, Karan Dalal, Chloe Hsu, Sanmi Koyejo, Carlos Guestrin, Xiaolong Wang, Tatsunori Hashimoto, and Xinlei Chen. Learning to (learn at test time). *arXiv preprint arXiv:2310.13807*, 2023. 6
- [45] Laurens Van der Maaten and Geoffrey Hinton. Visualizing data using t-sne. *Journal of Machine Learning Research*, 9(11):2579–2605, 2008. 8
- [46] Kaisiyuan Wang, Changcheng Liang, Hang Zhou, Jiayang Tang, Qianyi Wu, Dongliang He, Zhibin Hong, Jingtuo Liu, Errui Ding, Ziwei Liu, et al. Robust video portrait reenactment via personalized representation quantization. In *Proceedings of the AAAI Conference on Artificial Intelligence*, pages 2564–2572, 2023. 1
- [47] Kaisiyuan Wang, Hang Zhou, Qianyi Wu, Jiayang Tang, Zhiliang Xu, Borong Liang, Tianshu Hu, Errui Ding, Jingtuo Liu, Ziwei Liu, et al. Efficient video portrait reenactment via grid-based codebook. In *ACM SIGGRAPH 2023 Conference Proceedings*, pages 1–9, 2023. 1
- [48] Lizhen Wang, Xiaochen Zhao, Jingxiang Sun, Yuxiang Zhang, Hongwen Zhang, Tao Yu, and Yebin Liu. Styleavatar: Real-time photo-realistic portrait avatar from a single video. In *ACM SIGGRAPH 2023 Conference Proceedings*, pages 67:1–67:10, 2023. 2, 3, 4, 6
- [49] Yaohui Wang, Di Yang, Francois Bremond, and Antitza Dantcheva. Latent image animator: Learning to animate im-

- ages via latent space navigation. In *The International Conference on Learning Representations*, 2022. 1, 2
- [50] Olivia Wiles, A Koepke, and Andrew Zisserman. X2face: A network for controlling face generation using images, audio, and pose codes. In *Proceedings of the European Conference on Computer Vision*, pages 670–686, 2018. 2
- [51] Jinbo Xing, Menghan Xia, Yuechen Zhang, Xiaodong Cun, Jue Wang, and Tien-Tsin Wong. Codetalker: Speech-driven 3d facial animation with discrete motion prior. In *Proceedings of the IEEE/CVF Conference on Computer Vision and Pattern Recognition*, pages 12780–12790, 2023. 7
- [52] Chao Xu, Jiangning Zhang, Yue Han, Guanzhong Tian, Xianfang Zeng, Ying Tai, Yabiao Wang, Chengjie Wang, and Yong Liu. Designing one unified framework for high-fidelity face reenactment and swapping. In *European Conference on Computer Vision*, pages 54–71. Springer, 2022. 7
- [53] Yuelang Xu, Hongwen Zhang, Lizhen Wang, Xiaochen Zhao, Han Huang, Guojun Qi, and Yebin Liu. Latentavatar: Learning latent expression code for expressive neural head avatar. In *ACM SIGGRAPH 2023 Conference Proceedings*, pages 86:1–86:10, 2023. 1, 2
- [54] Kewei Yang, Kang Chen, Daoliang Guo, Song-Hai Zhang, Yuan-Chen Guo, and Weidong Zhang. Face2face ρ : Real-time high-resolution one-shot face reenactment. In *European Conference on Computer Vision*, pages 55–71. Springer, 2022. 7
- [55] Fei Yin, Yong Zhang, Xiaodong Cun, Mingdeng Cao, Yanbo Fan, Xuan Wang, Qingyan Bai, Baoyuan Wu, Jue Wang, and Yujiu Yang. Styleheat: One-shot high-resolution editable talking face generation via pre-trained stylegan. In *Proceedings of the European Conference on Computer Vision*, pages 85–101. Springer, 2022. 1, 2, 6, 7
- [56] Libing Zeng, Lele Chen, Yi Xu, and Nima Kalantari. Mystyle++: A controllable personalized generative prior. *arXiv preprint arXiv:2306.04865*, 2023. 2, 3
- [57] Fangneng Zhan, Yingchen Yu, Rongliang Wu, Jiahui Zhang, Shijian Lu, Lingjie Liu, Adam Kortylewski, Christian Theobalt, and Eric Xing. Multimodal image synthesis and editing: A survey and taxonomy. *IEEE Transactions on Pattern Analysis and Machine Intelligence*, 2023. 1
- [58] Bowen Zhang, Chenyang Qi, Pan Zhang, Bo Zhang, Hsiang-Tao Wu, Dong Chen, Qifeng Chen, Yong Wang, and Fang Wen. Metaportrait: Identity-preserving talking head generation with fast personalized adaptation. In *Proceedings of the IEEE/CVF Conference on Computer Vision and Pattern Recognition*, pages 22096–22105, 2023. 2
- [59] Han Zhang, Ian Goodfellow, Dimitris Metaxas, and Augustus Odena. Self-attention generative adversarial networks. In *International Conference on Machine Learning*, pages 7354–7363. PMLR, 2019. 2
- [60] Richard Zhang, Phillip Isola, Alexei A Efros, Eli Shechtman, and Oliver Wang. The unreasonable effectiveness of deep features as a perceptual metric. In *Proceedings of the IEEE Conference on Computer Vision and Pattern Recognition*, pages 586–595, 2018. 6
- [61] Wenxuan Zhang, Xiaodong Cun, Xuan Wang, Yong Zhang, Xi Shen, Yu Guo, Ying Shan, and Fei Wang. Sadtalker: Learning realistic 3d motion coefficients for stylized audio-driven single image talking face animation. In *Proceedings of the IEEE/CVF Conference on Computer Vision and Pattern Recognition*, pages 8652–8661, 2023. 7
- [62] Jian Zhao and Hui Zhang. Thin-plate spline motion model for image animation. In *Proceedings of the IEEE/CVF Conference on Computer Vision and Pattern Recognition*, pages 3657–3666, 2022. 2
- [63] Rui Zhen, Wenchao Song, Qiang He, Juan Cao, Lei Shi, and Jia Luo. Human-computer interaction system: A survey of talking-head generation. *Electronics*, 12(1):218, 2023. 1
- [64] Yufeng Zheng, Victoria Fernández Abrevaya, Marcel C Bühler, Xu Chen, Michael J Black, and Otmar Hilliges. Im avatar: Implicit morphable head avatars from videos. In *Proceedings of the IEEE/CVF Conference on Computer Vision and Pattern Recognition*, pages 13545–13555, 2022. 2, 4
- [65] Jun-Yan Zhu, Taesung Park, Phillip Isola, and Alexei A Efros. Unpaired image-to-image translation using cycle-consistent adversarial networks. In *Proceedings of the IEEE International Conference on Computer Vision*, pages 2223–2232, 2017. 4, 2

MyPortrait: Morphable Prior-Guided Personalized Portrait Generation

Supplementary Material

6. Dataset

The datasets used in the experiments are from Head2Head [8, 27] and NerFACE [11]. The monocular videos used in the experiments are shown in Tab. 6. We show the number of frames and the data source corresponding to each video. Some examples are shown in Fig. 10. Each image corresponds to a monocular video for neural portrait generation.

For the images used for experiments, we pre-crop the face images in the monocular video, keeping a fixed background and camera viewpoint. To extract the face parameters, we use some advanced face trackers. Specifically, we use DECA [10] to extract the pose coefficients $p \in R^6$ and expression coefficients $e \in R^{50}$ of the 3DMM [3, 4, 28, 36]. Then we use Gaze360 [24] to extract the gaze coefficients $g \in R^2$. In addition, we use DeepSpeech [1, 16] to extract audio features $a \in R^{16 \times 29}$ from the input audio.

7. Training Detail

During training, we define the monocular video used to provide personalized prior as *performing data*, and the dataset used to provide morphable prior as *auxiliary data*. Our framework uses the above data to perform a prior-guided two-stage training strategy as follows.

Taking the video-driven application as an example, in *stage I*, we use performing data to train the generator during reconstruction training. A total of 100,000 iterations are performed in this stage with the batch set to 16, using the Adam [26] optimizer with a learning rate of 0.0005. For the hyperparameters in the loss function, we set $\alpha_1 = 100$, $\alpha_2 = \alpha_3 = 0$, and $\alpha_4 = 1$. In *stage II*, we perform scalable training with both performing data and auxiliary data to train the generator and the discriminator. A total of 100,000 iterations are performed in this stage with the batch set to 8. We use the Adam optimizer where the learning rate is 0.0001 for the generator and 0.0004 for the discriminator. We set $\alpha_1 = 100$ and $\alpha_2 = \alpha_3 = \alpha_4 = 1$ for the loss function. For the audio-driven application, the audio-related network is trained with the generator.

Our method is implemented based on the Pytorch [35] framework, and trained on two GeForce RTX 3090. As shown in Fig. 11, we encode the face parameters using the positional encoding function, where $N_x = 10$ for the coordinate and $N_p = N_g = 4$ for the pose coefficients and gaze coefficients. In addition, the dimension of the learnable latent variable v is set to 32.

Label	Portrait	N	Data Source
(a)	ID.1	5513	NerFACE
(b)	ID.2	5518	
(c)	ID.3	5441	
(d)	Biden	5755	Head2Head
(e)	May	6050	
(f)	Obama	2218	
(g)	Trudeau	5035	
(h)	Tusk	3650	

Table 6. Illustration of the dataset used in the experiments. N defines the number of frames in a monocular video.

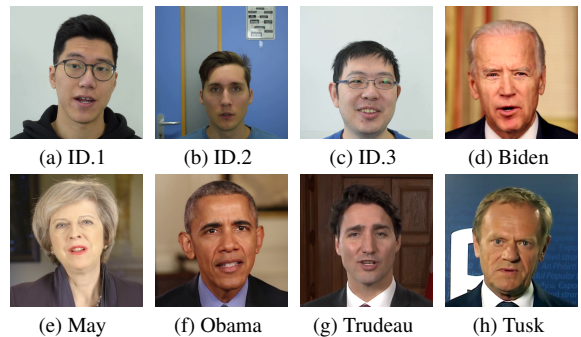


Figure 10. Example images of the dataset used in the experiments. Each image corresponds to a monocular video.

8. Network Structure

We use an efficient network architecture consisting of a 2D coordinate-based generator, a discriminator, and an optional audio-related network.

Generator. Our generator network includes a 2D coordinate-based multilayer perceptron (MLP) and a decoder based on convolutional neural networks (CNN). The MLP network consists of eight fully connected layers with all output dimensions of 128. The network structure of the MLP is illustrated in Fig. 11. In addition to predicting the feature vector based on the input parameter vector, MLP also predicts the pixel value to construct an improved reconstruction loss. For more details, please refer to DNP [9].

The CNN-based decoder contains six residual blocks and two upsampling blocks. Unlike DNP, we use bilinear interpolation rather than transposed convolution for upsampling because we observe that transposed convolution produces checkerboard artifacts [33]. By resizing the coordinate grid to 64×64 or 128×128 , we can generate images with resolutions of 256×256 or 512×512 , respectively. The network structure of the decoder is illustrated in Fig. 12.

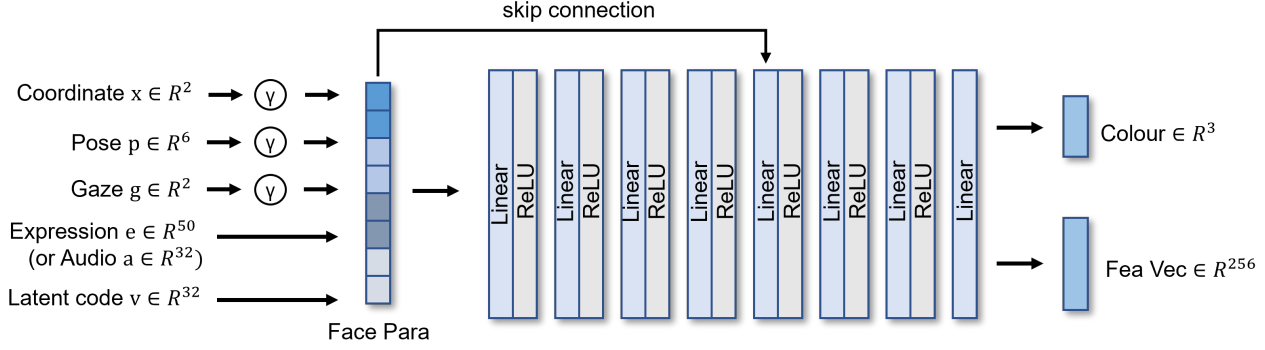


Figure 11. The architecture of the MLP network.

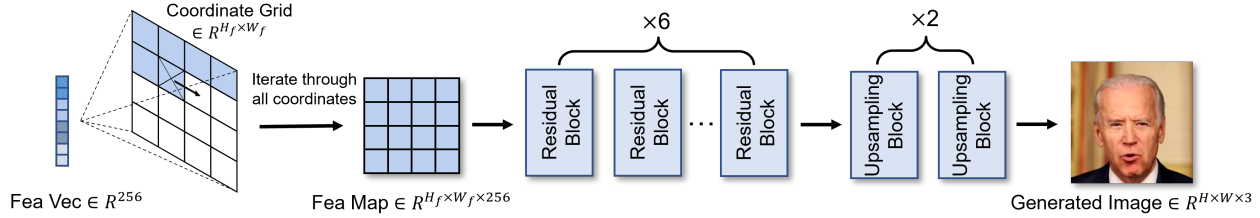


Figure 12. The architecture of the Decoder network.

Discriminator. We build the discriminator network based on PatchGANs [19, 65]. In addition, We use spectral normalization [31] to make the network stable during training.

Audio-related network. Following AD-NeRF [15], We first use DeepSpeech [1, 16] to transform speech into audio features with a window size of 16. Then we use a 1D-convolutional network and a self-attention [59] network to extract audio vectors of dimension 32. In the audio-driven task, the audio vector is fed into the generator network like other semantic parameters.

9. Discussion

Execution Speed. Benefiting from the simple network structure, our method enables real-time inference. The evaluation results of the execution speed are presented in Tab. 7. Our method takes only 14.3 milliseconds and 28.1 milliseconds to generate an image with a resolution of 256×256 and an image with a resolution of 512×512 , respectively. The experiment is performed on a GeForce RTX 3090.

Quality vs. Consistency. It should be noted that there are differences in the 3DMM neutral templates corresponding to different identities. Even if the 3DMM coefficients corresponding to the generated images are consistent with the driven data, it is not guaranteed that the expressions and poses of the generated images are exactly identical to those in the driven images. Therefore, instead of excessively pursuing such consistency, our method aligns the training and testing data at the expense of certain face parameter con-

Method	Param	256×256		512×512	
		Time	Fps	Time	Fps
Ours	7.6M	14.3	70.2	28.1	35.6

Table 7. The execution speed of our method. Time is reported in milliseconds (msec). Please note that all reported numbers refer to the forward pass time of models during inference, without considering data pre-processing.

sistency, effectively improving the generation quality. This assumption can be observed in the cross-reenactment experiments of the main text.